Hydrol. Earth Syst. Sci. Discuss., 12, 5703–5748, 2015
www.hydrol-earth-syst-sci-discuss.net/12/5703/2015/
doi:10.5194/hessd-12-5703-2015


Hydrology and Earth System Sciences
Discussions
Open Access



# Effective damage zone volume of fault zones and initial salinity distribution determine intensity of shallow aquifer salinization in geological underground utilization

**M. Langer[1], E. Tillner[1], T. Kempka[1], and M. Kühn[1,2]**

[1]GFZ German Research Centre for Geosciences, Sect. 5.3 – Hydrogeology, Telegrafenberg, 14473 Potsdam, Germany
[2]University of Potsdam, Institute of Earth- and Environmental Science, Am Neuen Palais 10, 14469 Potsdam, Germany

Received: 21 April 2015 – Accepted: 20 May 2015 – Published: 16 June 2015

Correspondence to: E. Tillner (elena.tillner@gfz-potsdam.de)

Published by Copernicus Publications on behalf of the European Geosciences Union.

## Abstract

Injection of fluids into deep saline aquifers causes a pore pressure increase in the storage formation, and thus displacement of resident brines. Via hydraulically conductive faults, brine may migrate upwards into shallower aquifers, and lead to unwanted salinization of potable groundwater resources. In the present study, we investigated different scenarios for a prospective storage site close to the city of Beeskow in the Northeast German Basin by using a 3-D regional scale model (100 km × 100 km × 1.34 km) that includes four ambient fault zones. The focus was on assessing the impact of fault length and the effect of an overlying secondary reservoir as well as model boundary conditions on the potential salinization of shallow groundwater resources. We employed numerical simulations of brine injection as a representative fluid using the simulator TOUGH2-MP.

Our simulation results demonstrate that pressure build-up within the reservoir determines the intensity and duration of fluid flow through the faults, and hence salinization of shallower aquifers. Application of different boundary conditions proved that these have a crucial impact on reservoir fluid displacement. If reservoir boundaries are closed, the fluid migrated upwards into the shallow aquifer, corresponds to the overall injected fluid mass. In that case, a short hydraulically conductive fault length and the presence of an overlying secondary reservoir leads only to retardation in brine displacement up to a factor of five and three, respectively. If the reservoir boundaries are open, salinization is considerably reduced: in the presence of a secondary reservoir, 33 % of equivalent brine mass migrates into the shallow aquifer, if all four faults are hydraulically open over their entire length, whereas the displaced equivalent brine mass is only 12 % for a single fault of two kilometres length. Taking into account the considered geological boundary conditions, the brine originates in maximum from the upper 4 to 298 m of the investigated faults. Hence, the initial salt–freshwater interface present in the fault is of high relevance for the resulting shallow aquifer salinization.

The present study demonstrates that the existence of hydraulically conductive faults is not necessarily an exclusion criterion for potential injection sites, because salinization of shallower aquifers strongly depends on initial salinity distribution, location of hydraulically conductive faults and their length as well as geological boundary conditions. These constraints are location specific, and need to be explored thoroughly in advance of any field activity. They provide the basis for scenario analyses and a reliable risk assessment.

## 1 Introduction

Carbon Capture and Storage (CCS) can contribute to the reduction of global anthropogenic carbon dioxide emissions. Different geological underground formations have been suggested as target storage sites, whereby deep saline aquifers provide the worldwide largest storage potential as part of the earth's widely distributed sedimentary basins (IPCC, 2005). Due to their extent and storage capacity, shallow aquifers in sedimentary basins comprise also considerable freshwater resources, which are of great importance for regional water supply. However, brine displacement due to the elevated pore pressure in the storage formation is one potential risk of $CO_2$ storage in saline aquifers. Saline fluids could reach shallower freshwater aquifers through different migration pathways, and significantly impair groundwater quality. Especially fault zones are of particular importance, as they form potential weakness zones within the host rock, and might act as large-scale permeable conduits penetrating several caprocks.

Displacement of brine and potential freshwater salinization as a result of $CO_2$ storage has been investigated in several studies. Table 1 summarizes the initial conditions and essential results of numerical simulations concerning this issue. The models applied are either synthetic (Oldenburg and Rinaldi, 2011; Birkholzer et al., 2011, 2009) or refer to a certain study area (Tillner et al., 2013; Zouh et al., 2010; Yamamoto et al., 2009; Nicot et al., 2008). Several studies examine pressure perturbation and resulting brine migration in a multi-barrier system without considering vertical conduits. It was shown that pressure build-up can be observed in a distance of more than 100 km from the injection zone (Birkholzer et al., 2009). Thereby, the choice of initial conditions and petrophysical parameters have a crucial impact on the pressure development, as demonstrated by two independent studies considering industrial-scale $CO_2$ injection in the Illinois Basin (Person et al., 2010; Zhou et al., 2010). After Person et al. (2010), the pressure perturbation is limited to a distance of about 25 km from the injection location for a total injection rate of 80 Mt $CO_2$ year$^{-1}$, whereas Zhou et al. (2010) simulated a pressure build-up as far as 300 km from the injection area (100 Mt $CO_2$ year$^{-1}$).

However, upward brine migration only occurs if pressure perturbation in the reservoir is large enough to overcome the weight of the fluid column in a vertical conduit. It further depends on magnitude of pressure increase, and whether brine is allowed to spread laterally in the upper aquifer, if a steady-state is reached or continuous flow develops (Oldenburg und Rinaldi, 2011; Birkholzer et al., 2011). Especially faults can represent vertical conduits, which may have an essential influence on groundwater flow and brine migration due to their extent and distribution in the Earth's upper crust. Nevertheless, a meaningful implementation of complex geological structures into a sufficiently discretised model grid is very difficult, especially at regional scale. Tillner et al. (2013) investigated the influence of permeable faults on brine displacement referring to a real study area. The authors simulated upward brine migration through complex fault systems depending on reservoir compartmentalisation and fault permeability, whereby faults were implemented by the virtual element approach (Nakaten et al., 2013). The results of Tillner et al. (2013) indicate that the degree of pressurization is the driving mechanism for brine migration, while permeability of fault zones does not influence salinization of shallower aquifers significantly. Their investigations focused on the prospective storage site Beeskow–Birkholz (in the following only referred to as Beeskow) in Northeast Germany, which is also considered in this work.

Here, we present a regional scale 3-D model with a simplified geometry, neglecting topographic variations while the four considered fault zones are implemented with their complex arrangement and curvature. Hence, the presumed simplifications should avoid numerical artefacts, and serve for improved comprehensibility of the relevant processes. In different leakage scenarios the effect of fault lengths, boundary conditions, and the presence of an overlying secondary reservoir on upward brine displacement as a result of fluid injection were assessed. The goal of this study was to deepen the general understanding of the underlying processes, as well as to characterize the impact of all investigated parameters to obtain site-specific findings on potential freshwater salinization.

## 2 Study area

The prospective $CO_2$ storage site is located 80 km southeast of Berlin in the Northeast German Basin (NEGB), which is part of the Southern Permian Basin (Fig. 1a). According to the estimated storage capacity, it was planned to inject 34 Mt $CO_2$ over a period of 20 years (1.7 Mt $CO_2$ year$^{-1}$) into a Mesozoic anticline structure at Beeskow (Vattenfall, 2009). Several sandstone formations of the Middle Buntsandstein, such as the Volpriehausen, Detfurth, and Hardegsen formations form potential reservoir rocks (Fig. 2a). They consist of basal sandstones and an alternating sequence of mudstones with sandy and silty layers (Vattenfall, 2010). The Detfurth Formation is characterized by the highest effective thickness of 23 m, and was therefore chosen as target storage horizon for $CO_2$ injection. Porous and fractured sediments of the lower Muschelkalk (Middle Triassic) represent a secondary suitable reservoir. A multi-barrier system of different cap rocks from the Upper Buntsandstein, the Middle and Upper Muschelkalk, as well as the Lower Keuper seals the Detfurth Formation and the overlying secondary reservoirs. The Rupelian clay (Oligocene, Upper Tertiary) forms a regional barrier between freshwater-bearing glacial sediments (Upper Tertiary and Quaternary) and the underlying saline aquifers. It is located at a depth between 150 and 200 m (Stackebrandt, 2010). Basal sandstones of the Rupelian with a thickness varying between 2.5 and 30 m are widespread, and mark the beginning of saltwater-bearing aquifers (Grube et al., 2010). During the latest three Pleistocene glacial phases, advances of the Scandinavian ice sheets locally formed deep-reaching erosion channels within the Rupelian clay. Hence, a hydraulic connection between deep saline aquifers and freshwater-bearing sediments exists in some parts of the area. Depending on the pressure potential, saline water could rise and mix with potable groundwater resources. As shown by Kempka et al. (2015), salt concentrations in the Quaternary deposits and fillings of the erosion channels can locally be larger than 10 $\text{g}\,\text{kg}^{-1}$.

The fault system of the study area consists of four regional fault zones comprising several individual faults. It divides the sedimentary cover of the study area into a regional block structure (Mittenwalde Block; Fig. 1b). The Lausitzer Abbruch and the Fuerstenwalde–Guben fault zones with NW–SE orientation, as well as the Tauer and the Potsdam fault zones striking NE–SW, enclose this compartment. All faults are normal faults with a steep inclination (between 67.8 and 74.3° in average). However, the Fuerstenwalde–Guben fault zone consists of several individual faults also characterized by reverse components of dip-slip. It has a total length of 120 km, and is characterized by an offset of a few hundred metres (Hotzan und Voss, 2013). The Lausitzer Abbruch fault zone dips NE, and shows displacements up to 1000 m (Beutler and Stackebrandt, 2012). This complex system was formed during the Variscan orogeny, whereby many faults were reactivated during the Alpine orogeny (Stackebrandt, 2010).

## 3 Geological model

We used the Petrel software package (Schlumberger, 2011) for the 3-D geological model construction and the subsequent gridding process, and the reservoir simulator TOUGH2-MP/ECO2N for 3-D multi-component flow simulations (Zhang et al., 2008; Pruess, 2005). All simulations were conducted on a high performance computing system with 256 cores. Finally, results were imported back into Petrel for visualization purposes.

### 3.1 Setup

The implementation of the 3-D geological model refers to the structural and geological characteristics of the study area as described above. It has a horizontal extent of 100 km × 100 km and a vertical thickness of 1340 m. Figure 2b shows the geological model with a regular lateral grid resolution of 250 m × 250 m. The vertical discretisation depends on the different model layers, and ranges between 10 and 19.9 m (Table 2). The model consists of up to three layers: the Rupelian basal sands as the uppermost shallow aquifer, the Muschelkalk Formation as an overlying secondary reservoir and the Detfurth Formation as lowermost reservoir. The Rupelian basal sands are 20 m thick and located at a depth of 110 m (Grube et al., 2010). The Lower Muschelkalk Formation is at 1025 m depth and has a thickness of 140 m, while the reservoir is at 1425 m depth with a thickness of 23 m (Tillner et al., 2013). The model is limited to the saline groundwater complex up to the Rupelian clay (situated above the Rupelian basal sands and not considered in the present model) as regional seal between salt and freshwater.

In a previous study, Kühn et al. (2011) investigated the influence of caprock permeabilities on shallower aquifer salinization at the prospective storage site Beeskow. Their results showed that for caprock permeabilities equal or lower than $10^{-17}$ $m^2$ no increase in salt concentration in formations above the reservoir has to be expected. In the present study, we assumed that the caprocks have lower permeabilities and therefore defined them as impermeable for fluid flow in all simulations, so that only the faults provide a hydraulic connection between the shallow aquifer and the reservoir. Thus, the elements of the faults as well as the different reservoir layers were “active” in our simulations, whereby the elements representing the caprocks were not considered. Depending on the different scenarios performed (varying fault length; with or without overlying secondary reservoir), the model consists of 635 508 to 1 811 473 active elements.

Within our model only the inner faults, which enclose the Mittenwalde Block were implemented as a representation of the entire fault zone (Fig. 1b). Thereby, fault related parameters were assigned to the elements located at the respective vertical fault plane. The fault element width of 250 m corresponds to the overall lateral grid resolution. This element width is relatively large but still realistic, since all regional fault zones consist of several individual faults and show considerable displacements. In general, fault offset is linked to the width of the damage zone (Faulkner et al., 2010; Mitchel and Faulkner, 2009; Wibberly et al., 2008). For example, faults with displacements between 10 m and 1000 m can have damage zone widths between tens and hundreds of metres. However, there exists no simple relationship, since the width of the damage zone is highly dependent on lithology, pressure, temperature, and strain rate during shear and potentially tensile deformation (Shipton et al., 2006). Due to the relatively steep inclination of all faults and to maintain maximum grid regularity, the dip angle was neglected in the present model and all faults were assumed to be strictly vertical. In the following, the Fuerstenwalde–Guben fault zone is addressed as Fault 1. The Potsdam, the Lausitzer Abbruch and the Tauer fault zones are referred to as Faults 2, 3 and 4, respectively (Fig. 1b).

The applied geological model was considered in the numerical simulations by simplifying the original topography of the formation tops and bases to focus the analysis on clearly identifiable effects of fault fluid flow.

### 3.2 Parameterization

All lithological units were parameterized according to Tillner et al. (2013) and Vattenfall (2009), with values derived from borehole data and literature and modelled as homogenous and isotropic. The Detfurth Formation has a permeability of 400 mD, while the overlying secondary reservoir (Muschelkalk Formation) is characterized by a permeability of 200 mD (Table 2). Porosity and permeability of the Rupelian basal sands were chosen according to Tesch (1987). Fault permeability was assumed higher than that of the host rock, because of fault-parallel permeability enhancement of the dam-





HESSD
12, 5703–5748, 2015

age zone due to the presence of a fracture network (Jourde et al., 2002; Caine et al., 1996). Thus, hydraulic properties of the faults were chosen to be in between of those of the Rupelian basal sands and the Detfurth Formation to allow for analysis of different time-dependent flow patterns (Table 2).

Because faults have a smaller offset at their boundaries, and consequently a less distinct damage zone, it was presumed that permeability declines in these areas. This was implemented into the model by using permeability multipliers in the respective elements. The permeability declines linearly towards the ends of the fault, applied to the first 15 % of its length. A lateral barrier for groundwater flow due to a low permeable fault core was not considered.

### 3.3 Initial and boundary conditions

In all investigated scenarios, Dirichlet boundary conditions were applied to the Rupelian basal sands. These were implemented by volume multipliers of $10^{10}$ at the boundary elements of each layer, so that the aquifer has quasi-infinite extension. The boundaries of the Detfurth and the Muschelkalk formations are either open (boundary element volume multiplication by $10^5$) or closed (no boundary element volume multiplication), depending on the investigated scenario. For the temperature distribution, a constant geothermal gradient of 30 °C km$^{-1}$ was used, starting from 15 °C at the model top. All simulations were performed at isothermal conditions resulting in a constant initial temperature in time and space. Studies suggest that the salinity in the Rupelian basal sands is between 0.8 and 3.8 % (Tesch, 1987), and increases with depth until full saturation in the Triassic layers (Hannemann and Schirrmeister, 1998). However, in the present models the transition between freshwater and brine was defined to be abrupt. Here, the Rupelian basal sands contain freshwater (zero salinity), whereas a salinity of 25 % was assigned to all underlying units. These conditions were chosen, as they lead to the maximum possible salinization in the uppermost aquifer, and thus represent the most unfavourable scenario for shallow aquifers under the given assumptions. Furthermore, a sharp salt–freshwater interface serves as a tracer boundary to visualize the





HESSD
12, 5703–5748, 2015

distribution of saline water within the shallow aquifer. All simulations were performed at hydrostatic pressure conditions. Considering the density of brine, pressure at the top of the Detfurth Formation at 1425 m depth is approximately 165 bar.

At the Beeskow storage site, it was planned to inject 34 Mt of $CO_2$ over a time span of 20 years into the Mesozoic anticline structure (Tillner et al., 2013). Instead of $CO_2$, the equivalent volume of brine was injected into the storage formation in the present study, because we assume that there is no substantial impact on resulting brine migration whether $CO_2$ or water is injected. Furthermore, with such a model we investigate injection-related brine displacement, and keep the findings transferable to various other types of subsurface storage. Considering a reservoir pressure of approximately 165 bar at the top of the Detfurth Formation and a temperature of 58 °C, the resulting $CO_2$ density is 668.5 $kg\,m^{-3}$ (Span and Wagner, 1996). Brine density sums up to 1175 $kg\,m^{-3}$, taking into account the salinity of 25 %. Thus, a volume equivalent mass of 59.76 Mt brine was injected into the storage formation, corresponding to a rate of 94.6 $kg\,s^{-1}$.

Fluid compressibility is considered in TOUGH2-MP/ECO2N by the use of its density changes, while brine densities are calculated for each element during the simulation. Pore compressibility causes a higher storage coefficient in the formations when pressure increases. Since our simulations should show the greatest possible effect on brine displacement, pore compressibility was neglected. Diffusion was also not considered, because it has an irrelevant effect within our model due to the chosen grid discretization and the long timespan it would require to observe substantial effects. If one takes into account a lateral element size of 250 m × 250 m, a fluid diffusion coefficient of $2 \times 10^{-9}\,m^2\,s^{-1}$ and a sharp freshwater–saltwater interface in the fault, it would take about 1 million years for the salinity front to propagate into a neighbouring element.





HESSD
12, 5703–5748, 2015

## 4 Set of scenarios

In total, 13 scenarios were selected to investigate the conditions for upward brine flow through the faults. Besides fault lengths, boundary conditions were varied and a potentially overlying secondary reservoir was considered. Scenarios are identified by the following abbreviations:

$$\text{Scenario} = F_n^{l} B_{\mathrm{O/C}} \mathrm{SR}_k$$

Where $F$ denotes fault with the coefficients l indicating the total fault length and $n$ the number of active faults. Further, the lateral boundary conditions ($B$) of both reservoirs can be either open (O) or closed (C). SR denotes that an overlying secondary reservoir exists and $k$ specifies the permeability of that reservoir. All simulated scenarios with their varying initial and boundary conditions are summarized in Table 3.

The base cases consist of two layers, while three different fault lengths were considered. Either all four fault zones with a total length of 193 km were assumed to be permeable, or Fault 1 was defined to be hydraulically conductive with a length of 60 km. In the third case, only a length of 2 km in the central part of Fault 1 was presumed to be open for fluid flow (Fig. 1b). All other parts of the faults were supposed to be impermeable, and therefore consist of inactive elements. These settings represent three different baseline examples, which should distinctly show differences for a better understanding of the relevant processes, and particularly define the possible spectrum of brine displacement. Further scenarios considered the three different fault lengths described above as well as the Muschelkalk Formation as an overlying secondary reservoir, since multi-barrier systems should preferably be chosen as potential $CO_2$ injection sites to minimize the risk of leakage. For all these cases, scenarios with both open and closed reservoir boundaries were examined to illustrate the entire range of a potential freshwater salinization depending on the given geological constraints.

Different fault permeabilities were not considered because previous simulations carried out with closed reservoir boundaries have primarily shown only a temporal effect





HESSD

12, 5703–5748, 2015

of fault permeability without any significant change in salinization. The mass of brine displaced into the shallow aquifer was the same in any case irrespective whether the fault permeability was higher, equal or lower than the permeability of the secondary reservoir (Fig. 3). A retardation in mass flow into the shallow aquifer by a factor of two was observed only for a fault permeability of 10 mD compared to the base case (700 mD), if all four faults were assumed to be hydraulically conductive. However, one simulation was applied in the present study to investigate the impact of permeability differences between reservoir and faults on upward brine migration taking into account open boundary conditions. In Scenario $F_{1-4}^{193\,\mathrm{km}}\,B_\mathrm{O}\mathrm{SR}_{2000\,\mathrm{mD}}$, the permeability of the Muschelkalk Formation was increased by one order of magnitude to 2000 mD, so that in contrast to all other scenarios, the permeability of the secondary reservoir is higher than the fault permeability.

# 5 Results

## 5.1 General outcomes

Some general outcomes are valid for all simulations. These results are presented first for a better understanding of the system. Figure 4 shows the mass flow in $\mathrm{kg\,s^{-1}}$ as an example for Scenario $F_{1-4}^{193\,\mathrm{km}}\,B_\mathrm{O}$ after 20 years, corresponding to the end of the injection period. At this time, reservoir pressures have reached their maximum, and thus effects on upward brine flow are most noticeable. An injection-related pattern in pressure distribution and fluid flow can be observed. Starting from the injection location, brine is displaced radially within the reservoir, and hence predominantly into parts of the faults close to the point of injection. Along the undulating Fault 3, which is located approximately 30 km away from the injection well, mass flow into parts facing towards the injection can be more than two times higher than into parts of the fault not facing the injection well (Fig. 4). However, the opposite case is noticeable in the shallow aquifer, where flow out of the fault into parts of the aquifer facing away from the injection (lower





HESSD
12, 5703–5748, 2015

pressures) is greater than into parts facing it (higher pressures). Hence, a redistribution of fluid flow occurs along the fault. Moreover, an asymmetric flow out of Fault 1 was observed within the Rupelian basal sands. Again, a higher mass flow out of the fault occurs into parts of the aquifer not facing the injection well since brine is displaced away from the point of highest pressurization. Consequently, salinities are higher normal to the fault in areas further away from the injection. This flow behaviour is valid for all scenarios and varies only in its intensity depending on pressure build-up and reduction.

Duration and intensity of fluid flow determines the spatial distribution of displaced saltwater. Maximum mass flow was observed along Fault 1 close to the injection decreasing towards the lateral boundaries of the fault. This pattern is reflected in the salinization of the freshwater aquifer, as shown in Fig. 5a as an example for Scenario $F_{1-4}^{193\,\mathrm{km}}\,B_\mathrm{C}$. A maximum salinity of 23 % is reached within the lower element layer of the shallow aquifer at the end of the injection period, whereas salinity varies only by 5 to 10 % at the fault edges. Brine migrates upwards through the fault as a result of the injection, and then spreads laterally within the Rupelian basal sands (Fig. 5b). Salinity levels are generally highest within the lower element layer, indicating that the denser saline water preferably spreads along the base of the aquifer. For the given Scenario $F_{1-4}^{193\,\mathrm{km}}\,B_\mathrm{C}$, the saltwater plume width in the Rupelian basal sands reaches a maximum of 2.4 km normal to the central part of Fault 1 and 1.2 km normal to the fault ends (Table 3). For the determination of the lateral distance affected by salinization, only salinities, which exceed 0.05 %, were considered. Due to the reduced brine displacement after the injection stop, a downward flow was observed. The more dense saline water accumulates at the base of the shallow aquifer. Moreover, a slight backflow into the fault occurs due to the increased weight of the water column as a result of the vertical brine displacement. Consequently, the salinity at the top element of the fault decreases by 1.5 to 23.5 % after a simulated time of 400 years (Fig. 5b), and the mass of brine within the fault slightly decreases due to the higher amount of freshwater, what can be observed in the relative mass change within the fault.





HESSD
12, 5703–5748, 2015

Effective damage zone volume of fault zones and initial salinity distribution

M. Langer et al.

Moreover, the maximum origin depth of the brine displaced into the shallow aquifer was estimated by calculating the fluid flow velocity at the top of the fault. The displaced brine derives from distinctly greater depths close to the injection than at the fault edges (Table 3), e.g. Scenario $F_{1-4}^{193\,\mathrm{km}}\,B_\mathrm{C}$ shows that close to the injection well, the displaced saline water mainly originates from the upper 30 m of the fault, whereas brine migrates from the upper 3 m at the fault edges only. In all simulations, displaced brine leading to a salinization of the shallow aquifer is displaced only from the upper part of the fault and not originating from the reservoir.

## 5.2 Fault length

### 5.2.1 Closed reservoir boundaries

Fig. 6a shows the distribution of the pressure increase within the upper element layer of the Detfurth Formation for different fault lengths and closed reservoir boundaries. We found the maximum pressure build-up at the injection point to be 89.9 bar for Scenario $F_1^{2\,\mathrm{km}}\,B_\mathrm{C}$, while pressure drops were observed in the surrounding of the faults. As expected, the highest pressure increase within the entire Detfurth Formation was encountered by implementing a hydraulic conductive fault segment with a length of two kilometres only. The pressure increases by 19.4 bar on average until the end of injection period in Scenario $F_1^{2\,\mathrm{km}}\,B_\mathrm{C}$, but only by 4.6 bar when all four faults are open for fluid flow (Table 3). The differences in pressurization of ca. one bar at the base of Fault 1 between scenarios $F_1^{60\,\mathrm{km}}\,B_\mathrm{C}$ and $F_{1-4}^{193\,\mathrm{km}}\,B_\mathrm{C}$ are low compared to the significant differences in total fault length. The pressure development at the base of Fault 1 shows that pressure increases until the injection stops after 20 years (Fig. 6b). In the following, the reduction of pressure is considerably faster, the greater the fault length. If all four faults are open (Scenario $F_{1-4}^{193\,\mathrm{km}}\,B_\mathrm{C}$), fluid flow into the shallow aquifer lasts for about 66 years, and is approximately five times faster than in Scenario $F_1^{2\,\mathrm{km}}\,B_\mathrm{C}$ (Table 3). For result evaluation, only a cumulative mass flow into the Rupelian basal sands above

$0.1\,kg\,s^{-1}$ was taken into account. To retrace and visualize the exchange of fluids between the different units, the relative mass change as a function of time was determined for the different geological units. Figure 7a illustrates that if the reservoir boundaries are closed, the mass of brine displaced into the shallow aquifer corresponds to the overall injected fluid mass. In this case, the open fault length has only a temporal effect on fluid migration.

A higher pressure build-up within the reservoir generally results in higher flow velocities out of the faults. Figure 8 shows the velocity profile through the lower element layer of the Rupelian basal sands. At the end of injection period, flow velocity out of the fault can be up to $29\,m\,yr^{-1}$ ($9.2 \times 10^{-7}\,m\,s^{-1}$) for a high pressure build-up due to a short fault length of two kilometres ($F_1^{2\,km}\,B_C$), while in scenarios $F_1^{60\,km}\,B_C$ and $F_{1-4}^{193\,km}\,B_C$ flow velocities range between 6.3 and $5.8\,m\,yr^{-1}$ ($1.8 \times 10^{-7}\,m\,s^{-1}$), respectively. Peaks in the velocity profile around the fault refer to the difference in fluid density between the displaced brine and residual freshwater within the aquifer. Maximum flow velocities were observed around Fault 1, which is located closest to the injection point. Further, velocity increases at the top of all other faults however, not as significantly as observed for Fault 1 (e.g. Fault 3, Fig. 8a). Flow velocities reach a maximum after 20 years. Subsequent to the injection stop, pressure reduction, and lower brine displacement are accompanied by decreasing flow velocities (Fig. 8b).

Freshwater salinization due to displaced brine only occurs locally around the faults. Spatial brine distribution in the Rupelian basal sands reaches a maximum lateral extent of 6.1 km, if a fault of two kilometres length serves as a conductive pathway (Table 3). When Fault 1 is completely open (Scenario $F_1^{60\,km}\,B_C$), brine spreads 2.4 km in maximum close to the injection area and only 1.5 km at the fault ends. Differences between the scenarios $F_1^{60\,km}\,B_C$ and $F_{1-4}^{193\,km}\,B_C$ are low, and mainly expressed by salt concentrations rather than lateral extension. Saline water, which migrates into the Rupelian basal sands, originates only from the fault. The depth of its origin mainly depends on the fault length: in Scenario $F_1^{2\,km}\,B_C$ brine is displaced into the shallow aquifer from the upper 298 m of the fault in maximum, while in Scenario $F_{1-4}^{193\,\mathrm{km}}\ B_\mathrm{C}$ saline water rises only 30 m (Table 3).

### 5.2.2 Open reservoir boundaries

If the reservoir boundaries are open, pressure build-up in the Detfurth Formation is considerably lower, while differences corresponding to the fault length still exist. The mean pressure increase within the reservoir is 2.1 bar, if all four faults are open ($F_{1-4}^{193\,\mathrm{km}}\ B_\mathrm{O}$), and hence only half as high as in the scenario with closed reservoir boundaries ($F_{1-4}^{193\,\mathrm{km}}\ B_\mathrm{C}$). In contrary to closed boundary conditions, pressure build-up at the model boundary does not occur. A pressure increase of at least one bar was observed in a maximum distance of 58 km ($F_{1}^{2\,\mathrm{km}}\ B_\mathrm{O}$) and 50 km ($F_{1-4}^{193\,\mathrm{km}}\ B_\mathrm{O}$), respectively, from the injection well. After the stop of injection, the pressure within the reservoir reduces substantially faster than under the assumption of closed reservoir boundaries (Fig. 6b). Hence, the duration of mass flow into the shallow aquifer is shorter for all three scenarios (Fig. 7a). Depending on the open fault length, a significant flow into the shallow aquifer occurs only for 31 years ($F_{1}^{2\,\mathrm{km}}\ B_\mathrm{O}$ and $F_{1}^{60\,\mathrm{km}}\ B_\mathrm{O}$) to 42 years ($F_{1-4}^{193\,\mathrm{km}}\ B_\mathrm{O}$). In contrast to closed reservoir boundaries, fluid flow into the Rupelian basal sands is maintained for a longer time period, if all four faults are hydraulically conductive compared to a single fault of only two kilometres length.

Due to lower reservoir pressures and the resulting shorter duration of mass flow, the total amount of brine, which is displaced into the shallow aquifer, is reduced in all cases with open reservoir boundaries. As Fig. 7b shows, 40 Mt brine reach the Rupelian basal sands when all four faults are open ($F_{1-4}^{193\,\mathrm{km}}\ B_\mathrm{O}$), corresponding to 66 % of displaced mass for the same fault length but closed reservoir boundaries ($F_{1-4}^{193\,\mathrm{km}}\ B_\mathrm{C}$). The displaced mass of brine is reduced by up to 30 % for a narrow fault of two kilometres length ($F_{1}^{2\,\mathrm{km}}\ B_\mathrm{O}$), because a major part of the fluid spreads within the laterally open reservoir (Fig. 7b). After the injection-related upward brine migration stops, a slight backward flow out of the shallow aquifer was additionally observed. Decreasing pressure causes





HESSD
12, 5703–5748, 2015

about 3.7 Mt dense fluid to flow out of the Rupelian basal sands back into the fault over a time period of 1500 years (Scenario $F_1^{2\,\mathrm{km}}\ B_\mathrm{O}$).

## 5.3 Overlying secondary reservoir

### 5.3.1 Closed reservoir boundaries

An overlying secondary reservoir has a strong impact on pressure build-up within the injection horizon. If all reservoir boundaries are closed, the mean pressure increase within the Detfurth Formation ranges from 15.9 bar ($F_1^{2\,\mathrm{km}}\ B_\mathrm{C}\mathrm{SR}_{200\,\mathrm{mD}}$) to 2.9 bar ($F_{1\text{–}4}^{193\,\mathrm{km}}\ B_\mathrm{C}\mathrm{SR}_{200\,\mathrm{mD}}$) in correspondence to 80 and 63 % of the pressure increase, respectively, without considering the overlying secondary reservoir (Table 3). After the injection period, reduction of the comparatively lower overpressures takes significantly longer, e.g. the mass flow into the Rupelian basal sands takes place for about 1050 years ($F_1^{2\,\mathrm{km}}\ B_\mathrm{C}\mathrm{SR}_{200\,\mathrm{mD}}$) and 225 years ($F_{1\text{–}4}^{193\,\mathrm{km}}\ B_\mathrm{C}\mathrm{SR}_{200\,\mathrm{mD}}$), which is more than three times longer compared to the models without a secondary reservoir. Figure 9 illustrates the explanation for this flow retardation: during the injection, fluid is displaced within the Detfurth Formation, and further through the faults into the Muschelkalk Formation (Fig. 9a). Due to the successive pressure reduction in both reservoirs, brine is transported out of the respective reservoir afterwards (Fig. 9b). This retardation can be clearly observed in the mass balances, comparing the displaced brine mass into the Rupelian basal sands for the scenarios with and without an overlying secondary reservoir (Fig. 9c). However, the overall displaced brine mass into the shallow aquifer is almost identical, when pressure comes to an equilibrium (Fig. 10). Nevertheless, for a short open fault of two kilometres ($F_1^{2\,\mathrm{km}}\ B_\mathrm{C}\mathrm{SR}_{200\,\mathrm{mD}}$) it takes a long time until the pressure conditions prior to injection are re-established, although pressure differences are already low.

Due to lower reservoir pressures, flow velocities are lower as well. This is particularly obvious for Scenario $F_1^{2\,\mathrm{km}}\ B_\mathrm{C}\mathrm{SR}_{200\,\mathrm{mD}}$, where flow velocity out of Fault 1 is halved at the end of the injection period compared to the scenario without the overlying sec-





HESSD
12, 5703–5748, 2015

ondary reservoir (Fig. 11). However, because the displaced brine mass becomes equal in both scenarios after a certain period of time, the area affected by salinity increase in the Rupelian basal sands is comparable to that observed in the simulations considering only two model layers (Table 3). Because of the delay in mass flow due to the existence of an overlying reservoir, the injection-related pattern occurs damped, and a more even distribution of saltwater in the shallow aquifer was observed. This is especially the case for the scenarios with greater fault length ($F_1^{60\,\mathrm{km}}$ $B_\mathrm{C}\mathrm{SR}_{200\,\mathrm{mD}}$ and $F_{1-4}^{193\,\mathrm{km}}$ $B_\mathrm{C}\mathrm{SR}_{200\,\mathrm{mD}}$): salinity and width of the displaced brine normal to the fault are slightly reduced closer to the injection well, while comparatively higher values can be observed at a greater distance to the point of injection.

### 5.3.2 Open reservoir boundaries

Open reservoir boundaries and an overlying secondary reservoir result in the lowest pressure build-up within the Detfurth Formation. The mean pressure increase in the reservoir ranges from 3.2 bar ($F_1^{2\,\mathrm{km}}$ $B_\mathrm{O}\mathrm{SR}_{200\,\mathrm{mD}}$) to 1.3 bar ($F_{1-4}^{193\,\mathrm{km}}$ $B_\mathrm{O}\mathrm{SR}_{200\,\mathrm{mD}}$), corresponding to 16 and 28 % of the pressure increase, respectively, without taking into account the overlying secondary reservoir (Table 3). A pressure increase of at least one bar was observed at a maximum distance of 55 km ($F_1^{2\,\mathrm{km}}$ $B_\mathrm{O}\mathrm{SR}_{200\,\mathrm{mD}}$) and 40 km ($F_{1-4}^{193\,\mathrm{km}}$ $B_\mathrm{O}\mathrm{SR}_{200\,\mathrm{mD}}$) from the injection well, depending on the open fault length. After the injection stop, pressure decreases much faster than in all other scenarios. The overlying secondary reservoir leads to a smaller retardation in fluid flow only, which is not comparable to the observed delay if reservoir boundaries are closed. Duration of mass flow into the shallow aquifer ranges between 31 years ($F_1^{2\,\mathrm{km}}$ $B_\mathrm{O}\mathrm{SR}_{200\,\mathrm{mD}}$) and 45 years ($F_{1-4}^{193\,\mathrm{km}}$ $B_\mathrm{O}\mathrm{SR}_{200\,\mathrm{mD}}$). A backflow out of the shallow aquifer was observed as well (Fig. 12).

The flow velocity out of the two kilometres long fault shows its maximum of 10 m yr$^{-1}$ at the end of the injection period. For the scenarios $F_1^{60\,\mathrm{km}}$ $B_\mathrm{O}\mathrm{SR}_{200\,\mathrm{mD}}$ and $F_{1-4}^{193\,\mathrm{km}}$ $B_\mathrm{O}\mathrm{SR}_{200\,\mathrm{mD}}$, flow velocities are only slightly lower, and decrease marginally





HESSD
12, 5703–5748, 2015

faster than in the simulations with closed boundaries (Fig. 11). The mass of brine displaced upward into the shallow aquifer is further reduced. Taking into account the backflow after 1000 years, only 7.2 Mt of brine are transported into the Rupelian basal sands for a fault length of two kilometres ($F_1^{2\,\mathrm{km}}\ B_\mathrm{O}\mathrm{SR}_{200\,\mathrm{mD}}$). This corresponds to 12 % of the mass which reaches the shallow aquifer when reservoir boundaries are closed and no secondary reservoir exists ($F_1^{2\,\mathrm{km}}\ B_\mathrm{C}$). The major part of the displaced fluid spreads within the laterally open Detfurth Formation. For greater fault lengths, also the mass brine migrating into the Rupelian basal sands is lower: here, only 27 % ($F_1^{60\,\mathrm{km}}\ B_\mathrm{O}\mathrm{SR}_{200\,\mathrm{mD}}$) and 33 % ($F_{1-4}^{193\,\mathrm{km}}\ B_\mathrm{O}\mathrm{SR}_{200\,\mathrm{mD}}$) of the injected mass is displaced into the freshwater aquifer, respectively (Fig. 12). For these scenarios, a higher amount of brine spreads within the Muschelkalk Formation.

Hence, due to the significantly lower brine displacement into the shallow aquifer, also the lateral brine extension is minor. In the Rupelian basal sands, the salinity increases up to a distance of 2.8 km around the fault with a length of two kilometres ($F_1^{2\,\mathrm{km}}\ B_\mathrm{O}\mathrm{SR}_{200\,\mathrm{mD}}$). This is less than half the extension compared to the scenario with closed reservoir boundaries and considering only two model layers ($F_1^{2\,\mathrm{km}}\ B_\mathrm{C}$). Moreover, the brine, which is displaced into the freshwater aquifer, originates from considerably shallower depths: for a fault length of two kilometres ($F_1^{2\,\mathrm{km}}\ B_\mathrm{O}\mathrm{SR}_{200\,\mathrm{mD}}$) the brine rises in the extreme from the upper 59 m of the fault. In the case with four open faults, ($F_{1-4}^{193\,\mathrm{km}}\ B_\mathrm{O}\mathrm{SR}_{200\,\mathrm{mD}}$) brine mainly originates from the upper 17 m of the faults.

### 5.4 Permeability differences between the fault and secondary reservoir

Our previous simulations demonstrate that if reservoir boundaries are closed, the permeability of the fault only has a temporal impact on fluid flow only, and the overall displaced brine mass into the freshwater aquifer becomes equal after a certain period. For this case, it is irrelevant if fault permeability is higher, equal or lower compared to the reservoir or aquifer. This is not the case if the reservoir boundaries are open (infinite aquifer).





HESSD
12, 5703–5748, 2015

In Scenario $F_{1-4}^{193\,\mathrm{km}}\ B_{\mathrm{O}}\mathrm{SR}_{2000\,\mathrm{mD}}$, the permeability of the Muschelkalk Formation is distinctly higher than that of the fault. The mean reservoir pressure increases by less than half (0.6 bar) compared to the scenario with a Muschelkalk Formation permeability of only 200 mD ($F_{1-4}^{193\,\mathrm{km}}\ B_{\mathrm{O}}\mathrm{SR}_{200\,\mathrm{mD}}$). In addition, the total duration of mass flow into the Rupelian basal sands is lowest with only 23 years compared to all other scenarios. However, in this scenario brine preferentially migrates into the permeable Muschelkalk Formation and not into the shallower aquifer. As illustrated in Fig. 13, most of the injected brine is displaced into the overlying secondary reservoir, and only 3.5 Mt remain in the Detfurth Formation. The mass of saline water transported into the Rupelian basal sands is only 5.5 Mt, corresponding to 9 % of the total injected mass. In consequence, salinization of the Rupelian basal sands is lowest, and the extent of the displaced brine smallest in this scenario compared to all others (Table 3). Moreover, the fluid that is displaced into the shallow aquifer originates solely from the upper 4 m of the faults.

## 6 Discussion

The analysis of all scenarios provides both, general outcomes for a better understanding of the relevant processes and the impact of all investigated parameters as well as site-specific findings. In a previous study, Tillner et al. (2013) demonstrated that pressure build-up in the reservoir is the driving factor in upwards brine migration: larger pressure build-up leads to stronger brine displacement, and consequently higher salinities in shallow aquifers. Our simulations confirm these observations. Moreover, we have shown that the magnitude of pressure build-up induced by fluid injection and its release strongly depends on the choice of lateral boundary conditions, the effective damage zone volume of faults and the presence of secondary reservoirs. The maximum pressure increase of 19.4 bar in average within the reservoir occurs if the reservoir boundaries are closed, no overlying secondary reservoir exists, and the hydraulically conductive fault segment is short ($F_1^{2\,\mathrm{km}}\ B_{\mathrm{C}}$). This results in the highest observed flow





HESSD
12, 5703–5748, 2015

velocities of 29 $\mathrm{m\,yr^{-1}}$ for Fault 1. Consequently, the displaced brine spreads 6.1 km laterally around the fault within the shallow aquifer in the extreme. Moreover, the spatial distribution of pressure build-up leads to an injection-related pattern in fluid flow, resulting in higher salinities within the Rupelian basal sands above fault intervals, which are located closer to the injection well. However, we neglected pore compressibility in our models to maximize pressurization and subsequent brine displacement. Considering pore compressibility, would lead to a slight reduction in injection-related pressure-build up due to higher storage coefficients in the formations, and consequently to less intense brine displacement during the injection period.

All simulations with closed reservoir boundaries that correspond to a spatially restricted reservoir further show that the mass of brine displaced into the shallow aquifer corresponds to the overall injected mass. For that reason, fluid flow persists until the injection-related overpressure within the reservoirs is completely vanished. Hence, only a temporal effect on upward brine migration depending on fault length and the presence of an overlying reservoir was observed in this case. For a fault segment of two kilometres length ($F_1^{2\,\mathrm{km}}\ B_\mathrm{C}$) the flow into the shallow aquifer can last up to five times longer than for the scenario with four open faults ($F_{1\text{–}4}^{193\,\mathrm{km}}\ B_\mathrm{C}$). Thereby, the presence of an overlying secondary reservoir results in fluid flow retardation by factor 3.1 to 3.4 in the scenarios $F_1^{2\,\mathrm{km}}\ B_\mathrm{C}\mathrm{SR}_{200\,\mathrm{mD}}$ and $F_{1\text{–}4}^{193\,\mathrm{km}}\ B_\mathrm{C}\mathrm{SR}_{200\,\mathrm{mD}}$, respectively. Open reservoir boundaries represent an aquifer with a quasi-infinite extension and allow lateral pressure dissipation. As a result, substantially lower pressures within the Detfurth Formation and a reduction of shallow aquifer salinization can be observed. Consequently, only 66 % of the brine mass is displaced into the shallow aquifer assuming four open faults ($F_{1\text{–}4}^{193\,\mathrm{km}}\ B_\mathrm{O}$) and about 30 % in the two kilometres single fault case ($F_1^{2\,\mathrm{km}}\ B_\mathrm{O}$) in comparison to the corresponding scenarios with closed faults. The presence of an overlying secondary reservoir leads to an additional decrease in salinity: 33 and 12 % of equivalent brine mass migrates into the shallow aquifer in the scenarios $F_{1\text{–}4}^{193\,\mathrm{km}}\ B_\mathrm{O}\mathrm{SR}_{200\,\mathrm{mD}}$ and $F_1^{2\,\mathrm{km}}\ B_\mathrm{O}\mathrm{SR}_{200\,\mathrm{mD}}$, respectively. These results illustrate the relevance of represent-





HESSD
12, 5703–5748, 2015

ing the site-specific geological conditions as close as possible, as previously proposed by e.g. Cavanagh and Wildgust (2011).

As mentioned above, the results of the investigated scenarios emphasize that also the effective volume of the hydraulically conductive length of the fault zones has an important influence on pressure build-up and release in geological underground utilization. Depending on the fault length, also the duration and intensity of the mass flow varies, in turn determining the overall salinization of a shallow aquifer. A short hydraulically conductive fault segment leads to higher reservoir pressures and a wider salinization locally around the fault ($F_1^{2\,\mathrm{km}}$) than a fault that is open over its entire length ($F_{1-4}^{193\,\mathrm{km}}$), because pressure dissipation occurs across a smaller area. Based on our definition, that the fault is either permeable (open) or impermeable (closed) for fluid flow, the location of potential salinization is pre-determined. Hence, the open fault length affects both, the location and degree of the occurring salinization. Moreover, these influences correspond not only to fault length, but also to fault width, since porosity was maintained constant during all our simulations. Thus, the effective damage zone volume of hydraulically conductive faults is relevant for the simulation outcome.

Tillner et al. (2013) showed that the permeability of fault zones only has a minor impact and does not influence salinization of shallower aquifers significantly. The authors considered mainly fault permeabilities higher than that of the reservoirs. Our previous simulations have also primarily shown a temporal effect of fault permeability without any significant change in salinization assuming closed reservoir boundaries. Furthermore, our results demonstrate that the relation between fault and reservoir permeability has a crucial impact on salinization of upper aquifers assuming a laterally infinite reservoir extension. In Scenario $F_{1-4}^{193\,\mathrm{km}}\ B_\mathrm{O}\mathrm{SR}_{2000\,\mathrm{mD}}$, it is shown that fault permeability lower compared to that of the secondary reservoir, determines the preferential brine flow direction. If permeability of the secondary reservoir exceeds that of the fault, the mass of brine migrating into the Rupelian basal sands is only around a quarter of that observed in the opposite case ($F_{1-4}^{193\,\mathrm{km}}\ B_\mathrm{O}\mathrm{SR}_{200\,\mathrm{mD}}$).





HESSD
12, 5703–5748, 2015

Simulations taking into account an overlying secondary reservoir result in considerably lower pressures in the storage reservoir. Moreover, a dampening effect on salinization of the shallow aquifer occurs, because fluid is partially displaced into this layer, and thus further brine displacement upward the fault is reduced. Hence, it can be assumed, that the potential salinization of a shallow aquifer is lowered with each aquifer lying in between the reservoir and the shallow aquifer. Similar results were achieved by an analytical approach of Nordbotten et al. (2004), investigating fluid leakage through wells in a multi-barrier system with up to 12 aquifers. The authors observed a successive decrease in intensity of fluid upward displacement, caused by loss of fluid into the intermediate aquifer layers, what consequently highly reduces leakage in the shallowest aquifer. Birkholzer et al. (2009) also showed, however, without considering a vertical conduit that the amount of fluid displaced into formations above the reservoir, decreases upwards due to the attenuation capacity of the overlying rocks.

For the given geological conditions and the assumed injection rate, the fluid displaced into the shallow aquifer originates solely from the upper part of the fault. Depending on the scenario, brine displaced into the shallow aquifer originates from the upper 4 m ($F_{1-4}^{193\,\mathrm{km}}$ $B_{\mathrm{O}}\mathrm{SR}_{2000\,\mathrm{mD}}$) to 298 m ($F_1^{2\,\mathrm{km}}$ $B_{\mathrm{C}}$) of the part of Fault 1 lying close to the injection, while the depth of brine origin is substantially reduced up to less than 1 m at fault edges. Consequently, the initial distribution of salinity within the fault is crucial for the assessment of shallow aquifer salinization. Our simulations with a fault fully saturated with brine correspond to an end member resulting in a maximum freshwater salinization. In this case, a small conductive fault segment would lead to higher salinities and a greater lateral propagation of the saltwater, while faults with a great effective damage zone volume lead to a more distributed salinization but lower spatial widths of the saltwater distribution. If, however, a gradient in salinity exists or the salt–freshwater interface lies below the depth, from which brine is displaced into the shallow aquifer, freshwater salinization is considerably reduced or might not occur. Nevertheless, if the displaced brine reaches the shallow groundwater system it spreads preferentially at the aquifer base, as indicated by considerably higher salinities at the lower element



Discussion Paper | Discussion Paper | Discussion Paper | Discussion Paper |

HESSD

12, 5703–5748, 2015

Effective damage zone volume of fault zones and initial salinity distribution

M. Langer et al.

layer in the Rupelian basal sands. These results are in agreement with the findings of Oldenburg and Rinaldi (2011).

Our simulation results also show that the duration of brine displacement into the shallow aquifer is not limited to the injection period. Even in the scenario assuming open reservoir boundaries and four hydraulically conductive faults ($F_{1-4}^{193\,\text{km}}$ $B_O$), both supporting a fast pressure reduction, brine displacement into the shallow aquifer persists for more than twice the injection period. This illustrates the relevance of considering also the post-injection phase in salinization assessments, since neglecting the ongoing fluid flow processes could lead to an underestimation of the potential freshwater salinization. Moreover, it is important to recognize further post-injection processes, as the observed density-driven flow out of the shallow aquifer back into the faults occurring due to the increased weight of the water column.

Finally, we can complement our general findings with site-specific insights: for the study area, the presence of overlying reservoirs, represented by the Hardegsen, Muschelkalk and Stuttgart formations, as well as the initial gradient in salinity are known. This gradient reduces the potential salinization, because the fluids displaced into the Rupelian basal sands would be of essentially lower salinity than assumed in our simulations. Based on these results, it can be concluded that for a large effective damage zone volume (as in Scenario $F_{1-4}^{193\,\text{km}}$), shallow aquifer salinization is estimated as low, even if fluid is displaced over extensive areas into the Rupelian basal sands, because the origin depth of these fluids lies in maximum only a few decametres below the shallow aquifer. At the same time, local and very permeable segments of the fault (as in Scenario $F_1^{2\,\text{km}}$) affect a higher vertical distance by upward brine migration, resulting in a higher potential for possible freshwater salinization. Furthermore, according to the present study, we are convinced that the three interlayered reservoirs would dampen brine displacement into the shallow aquifers, because fluids would be partly displaced into these layers instead of further migrating upwards.





HESSD
12, 5703–5748, 2015

## 7 Summary and conclusions

In the present study, a regional scale 3-D model (100 km × 100 km × 1.34 km) of the prospective storage site Beeskow in the Northeast German Basin was implemented to investigate a potential salinization of potable groundwater resources due to upward brine migration through hydraulically conductive fault zones. For that purpose, 13 scenarios were examined to assess the impact of fault lengths between 2 and 193 km in the vicinity and around the injection site. Further, the effects of an overlying secondary reservoir as well as the geological boundary conditions on the salinization of a shallow aquifer were evaluated.

We have shown that pressure build-up and its development over time within the reservoir determine the intensity and duration of fluid flow through the faults, and thereby the salinization of shallower aquifers. Thereby, the total mass of brine displaced into the uppermost aquifer essentially depends on the chosen geological boundary conditions: if reservoir boundaries are closed, representing a spatially restricted reservoir, the fluids migrating into the shallow aquifer correspond to the overall injected fluid mass (assuming zero pore compressibility). Only a temporal effect was observed on the retardation of fluid flow for shorter open fault lengths and the presence of an overlying secondary reservoir. If reservoir boundaries are open, corresponding to an aquifer with quasi-infinite extension, freshwater salinization is considerably reduced. With a secondary reservoir, only 12 % of equivalent brine mass migrates into the shallow aquifer for a hydraulically open fault segment of two kilometres.

The initial salinity distribution and location of the fresh–saltwater interface within the upper part of the fault is of high relevance for risk assessment related to salinization in shallow aquifers. For the considered geological conditions, the fluid displaced into the uppermost aquifer originates in maximum from the upper 4 to 298 m of the investigated faults. Hence, if the salt–freshwater interface lies below this depth, no salinization is likely to occur, since only freshwater would be displaced into the shallow aquifer. In general, the potential of freshwater salinization is small for greater fault lengths, because





HESSD
12, 5703–5748, 2015

the origin depth of the fluids displaced into the shallow aquifer lies a few decametres below the shallow aquifer in maximum, due to lower pressure build-up. Short and very permeable fault segments may have a higher salinization potential due to a larger vertical distance affected by fluid displacement. Moreover, it can be concluded that aquifers lying in between a deep reservoir and the shallow aquifer, like in a multi-barrier system, further diminish salinization of the shallow aquifer, because saline fluids from the faults are partly displaced into these layers.

The unknown effective damage zone volume of fault zones is the greatest uncertainty in estimating the potential salinization of shallow freshwater resources. Hence, a site-specific assessment of a possible freshwater salinization requires a sensitivity analysis with varying effective damage zone volumes of the present faults. Furthermore, the injection-induced pressure increase generally results in a decrease in effective stresses. In this context, coupled hydro-mechanical simulations support estimating the (re-)activation potential of faults by shear and/or tensile failure as well as fault fill property changes resulting from volumetric strain increments (Magri et al., 2013; Röhmann et al., 2013; Cappa and Rutqvist, 2011; Chin et al., 2000). With respect to our simulation results, we conclude that hydraulically conductive fault zones do not necessarily lead to freshwater salinization owing to upward fluid displacement. This principally depends on the initial salinity distribution, effective volume of the fault damage zone and the geological boundary conditions. We showed that numerical simulations are applicable to obtain site-specific insights on the relevant factors affecting dynamic fluid flow processes. Since every field site is very complex and especially most of the heterogeneities in the subsurface are unknown, we focused here on selected end members to estimate the site-specific bandwidth of the potential salinization. Field explorations should be employed prior to any underground utilization to obtain more accurate data, especially on the effective damage zone volume of present fault zones as well as the initial salinity distribution.

*Acknowledgements.* We would like to thank our colleagues Benjamin Nakaten and Marco De Lucia (GFZ German Research Centre for Geosciences) for technical support and constructive





HESSD
12, 5703–5748, 2015

comments.

The article processing charges for this open-access publication were covered by a Research Centre of the Helmholtz Association.

## References

Beutler, G. and Stackebrandt, W.: The tectonic pattern of the sedimentary cover of Brandenburg – suggestion for a uniform nomenclature, Brandenburgische Geowissenschaftliche Beiträge, Kleinmachnow, 19, 93–109, 2012, (in German).

Birkholzer, J. T., Zhou, Q., and Tsang, C.-F.: Large-scale impact of $CO_2$ storage in deep saline aquifers: a sensitivity study on pressure response in stratified systems, Int. J. Greenh. Gas Con., 3, 181–194, doi:10.1016/j.ijggc.2008.08.002, 2009.

Birkholzer, J. T., Nicot, J. P., Oldenburg, C. M., Zhou, Q., Kraemer, S., and Bandilla, K.: Brine flow up a well caused by pressure perturbation from geologic carbon sequestration: static and dynamic evaluations, Int. J. Greenh. Gas Con., 5, 850–861, doi:10.1016/j.ijggc.2011.01.003, 2011.

Caine, J., Evans, J., and Forster, C.: Fault zone architecture and permeability structure, Geology, 24, 1025–1028, doi:10.1130/0091-7613(1996)024<1025:FZAAPS>2.3.CO;2, 1996.

Cappa, F. and Rutqvist, J.: Modeling of coupled deformation and permeability evolution during fault reactivation induced by deep underground injection of $CO_2$, Int. J. Greenh. Gas Con., 5, 336–346, doi:10.1016/j.ijggc.2010.08.005, 2011.

Cavanagh, A. and Wildgust, N.: Pressurization and brine displacement issues for deep saline formation $CO_2$ storage, Energy Procedia, 4, 4814–4821, doi:10.1016/j.egypro.2011.02.447, 2011.

Chin, L. Y., Raghavan, R., and Thomas, L. K.: Fully coupled geomechanics and fluid-flow analysis of wells with stress-dependent permeability, SPE J., 5, 32–45, Paper 58968, doi:10.2118/58968-PA, 2000.

Faulkner, D. R., Jackson, C. A. L., Lunn, R. J., Schlische, R. W., Shipton, Z. K., Wibberley, C. A. J., and Withjack, M. O.: A review of recent developments concerning the structure, mechanics and fluid flow properties of fault zones, J. Struct. Geol., 32, 1557–1575, doi:10.1016/j.jsg.2010.06.009, 2010.

Grube, A., Wichmann, K., Hahn, J., and Nachtigall, K.: Geogene Grundwasserversalzung in den Poren-Grundwasserleitern Norddeutschlands und ihre Bedeutung für die Wasserwirtschaft, Band 9, DVGW-Technologiezentrum Wasser, Karlsruhe, 2000, (in German).

Hannemann, M. and Schirrmeister, W.: Paleohydrological basics of the development of the boundary of fresh and salt water as well as of the salt water-outlets in Brandenburg, Brandenburgische Geowissenschaftliche Beiträge, Kleinmachnow, 5, 61–72, 1998, (in German).

Hotzan, G. and Voss, T.: Complex hydrogeochemic-genetic mapping for evaluation of the endangerment of pleistocene and tertiary aquifers by saline waters in the region Storkow-Frankfurt (Oder)-Eisenhüttenstadt, Brandenburgische Geowissenschaftliche Beiträge, Kleinmachnow, 20, 62–82, 2013, (in German).

IPCC – Metz, B., Davidson, O., de Coninck, H. C., Loos, M., and Meyer, L. A. (Eds.): IPCC Special Report on Carbon Dioxide Capture and Storage, Prepared by Working Group III of the Intergovernmental Panel on Climate Change, Cambridge University Press, New York, 431 pp., 2005.

Jourde, H., Flodin, E., Aydin, A., Durlovsky, L., and Wen, X.: Computing permeability of fault zones in eolian sandstone from outcrop measurements, AAPG Bull., 86, 1187–1200, doi:10.1306/61EEDC4C-173E-11D7-8645000102C1865D, 2002.

Kempka, T., Herd, R., Huenges, E., Endler, R., Jahnke, C., Janetz, S., Jolie, E., Kühn, M., Magri, F., Meinert, P., Moeck, I., Möller, M., Muñoz, G., Ritter, O., Schafrik, W., Schmidt-Hattenberger, C., Tillner, E., Voigt, H.-J., and Zimmermann, G.: Joint research project Brine: carbon dioxide storage in eastern Brandenburg: implications for synergetic geothermal heat recovery and conceptualization of an early warning system against freshwater salinization, in: Geological Storage of $CO_2$ – Long Term Security Aspects, edited by: Liebscher, A. and Münch, U., GEOTECHNOLOGIEN Science Report No.22, Advanced Technologies in Earth Sciences, Springer International Publishing, Cham, Switzerland, 139–166, 2015.

Kühn, M., Kempka, T., and Jolie, E.: Evaluation of potential pressurisation and salinisation of freshwater reservoirs by brine migration as a result of geological $CO_2$ storage, 4th International Conference GeoProc2011, Perth, Australia, 6–9 July 2011, Paper No: GP026, 1–9, 2011.

Magri, F., Tillner, E., Wang, W., Watanabe, N., Zimmermann, G., and Kempka, T.: 3D hydro-mechanical scenario analysis to evaluate changes of the recent stress field as a result of geological $CO_2$ storage, Energy Procedia, 40, 375–383, doi:10.1016/j.egypro.2013.08.043, 2013.





HESSD

12, 5703–5748, 2015

Effective damage zone volume of fault zones and initial salinity distribution

M. Langer et al.

Mitchell, T. and Faulkner, D.: The nature and origin of off-fault damage surrounding strike-slip fault zones with a wide range of displacements: a field study from the Atacama fault system, northern Chile, J. Struct. Geol., 31, 802–816, doi:10.1016/j.jsg.2009.05.002, 2009.

Nakaten, B., Tillner, E., and Kempka, T.: Virtual elements for representation of faults, cracks and hydraulic fractures in dynamic flow simulations, Energy Procedia, 40, 447–453, doi:10.1016/j.egypro.2013.08.051, 2013.

Nicot, J.: Evaluation of large-scale $CO_2$ storage on fresh-water sections of aquifers: an example from the Texas Gulf Coast Basin, Int. J. Greenh. Gas Con., 2, 582–593, doi:10.1016/j.ijggc.2008.03.004, 2008.

Nordbotten, J. M., Celia, M. A., and Bachu, S.: Analytical solutions for leakage rates through abandoned wells, Water Resour. Res., 40, W04204, doi:10.1029/2003WR002997, 2004.

Person, M., Banerjee, A., Rupp, J., Medina, C., Lichtner, P., Gable, C., Pawar, R., Celia, M., McIntosh, J., and Bense, V.: Assessment of basin-scale hydrologic impacts of $CO_2$ sequestration, Illinois basin, Int. J. Greenh. Gas Con., 4, 840–854, doi:10.1016/j.ijggc.2010.04.004, 2010.

Oldenburg, C. and Rinaldi, A.: Buoyancy effects on upward brine displacement caused by $CO_2$ injection, Transport Porous Med., 87, 525–550, doi:10.1007/s11242-010-9699-0, 2011.

Pruess, K.: ECO2N: A TOUGH2 Fluid Property Module for Mixtures of Water, NaCl, and $CO_2$, Lawrence Berkeley National Laboratory, Berkeley, CA, 66 pp., 2005.

Röhmann, L., Tillner, E., Magri, F., Kühn, M., and Kempka, T.: Fault reactivation and ground surface uplift assessment at a prospective German $CO_2$ storage site, Energy Procedia, 40, 437–446, doi:10.1016/j.egypro.2013.08.050, 2013.

Schlumberger: Petrel Seismic-to-Evaluation Software, Version 2011.2.7, 2011.

Shipton, Z., Soden, A., Kirkpatrick, J., Bright, A., and Lunn, R.: How thick is a fault? Fault displacement-thickness scaling revisited, in: Earthquakes: Radiated Energy and the Physics of Faulting, American Geophysical Union, Washington DC, 193–198, doi:10.1029/170GM19, 2006.

Span, R. and Wagner, W.: A new equation of state for carbon dioxide covering the fluid region from the triple-point temperature to 1100 K at pressures up to 800 MPa, J. Phys. Chem. Ref. Data, 25, 1509–1596, doi:10.1063/1.555991, 1996.

Stackebrandt, W.: Outline of the geological setting of Brandenburg, Brandenburgische Geowissenschaftliche Beiträge, Kleinmachnow, 5, 3–7, 2010, (in German).

Tesch, J.: Hydrogeological report with groundwater reserve estimation, VE 1987 – VED Hydrogeologie, BT Berlin, Berlin, 1987, (in German, unpublished).
Tillner, E., Kempka, T., Nakaten, B., and Kühn, M.: Brine migration through fault zones: 3D numerical simulations for a prospective $CO_2$ storage site in Northeast Germany, Int. J. Greenh. Gas Con., 19, 689–703, doi:10.1016/j.ijggc.2013.03.012, 2013.
Vattenfall: Antrag auf Erteilung einer Erlaubnis zur Aufsuchung bergfreier Bodenschätze zu gewerblichen Zwecken, available at: http://www.lbgr.brandenburg.de/media_fast/4055/Antrag%200_Aufsuchung%20bergfreier%20Bodensch%C3%A4tze_Bkh_20090306.15564291.pdf, 12 pp., (last access: 18 December 2014), 2009, (in German).
Vattenfall: Hauptbetriebsplan – Aufsuchungsarbeiten in Bezug auf den bergfreien Bodenschatz Sole im Erlaubnisfeld Birkholz-Beeskow, 28 pp., available at: http://www.lbgr.brandenburg.de/media_fast/4055/Bkh_HBP_Finale.pdf, (last access: 18 December 2014), 2010 (in German).
Wibberley, C. A. J., Yielding, G., and Toro, G.: Recent advances in the understanding of fault zone internal structure: a review, in: The Internal Structure of Fault Zones: Implications for Mechanical and Fluid-Flow Properties, Geological Society of London, London, 5–33, doi:10.1144/SP299.2, 2008.
Yamamoto, H., Zhang, K., Karasakib, K., Marui, A., Hitoshi Uehara, H., and Nishikawa, N.: Numerical investigation concerning the impact of $CO_2$ geologic storage on regional groundwater flow, Int. J. Greenh. Gas Con., 3, 586–599, doi:10.1016/j.ijggc.2009.04.007, 2009.
Zhang, K., Wu, Y. S., and Pruess, K.: User's Guide for TOUGH2-MP – A Massively Parallel Version of the TOUGH2 Code, Earth Sciences Division, Lawrence Berkeley National Laboratory, Berkeley, 108 pp., 2008.
Zhou, Q., Birkholzer, J., Mehnert, E., Lin, Y., and Zhang, K.: Modelling basin- and plume-scale processes of $CO_2$ storage for full-scale deployment, Ground Water, 48, 494–514, doi:10.1111/j.1745-6584.2009.00657.x, 2010.





HESSD
12, 5703–5748, 2015

Effective damage zone volume of fault zones and initial salinity distribution

M. Langer et al.

Title Page
Abstract | Introduction
Conclusions | References
Tables | Figures
◂◂ | ▸▸
◂ | ▸
Back | Close
Full Screen / Esc
Printer-friendly Version
Interactive Discussion

**Table 1.** Summary of numerical simulations of brine migration resulting from $CO_2$ injection.

| Authors | Study area and model extend | Reservoir boundaries | Simulator | Injection rate of $CO_2$ and duration | Injected fluid | Objectives | Results |
|---|---|---|---|---|---|---|---|
| Birkholzer et al., 2009 | • synthetic<br>• 125 000 $km^2$ (radial symmetric) | open | TOUGH2/ECO2N | 1.52 $Mt\,yr^{-1}$ over 30 years | $CO_2$ | Pressure build-up and brine migration in the reservoir and through low permeable caprocks | • Considerable pressure build-up in a distance of > 100 km from injection zone<br>• Vertical brine migration through a sequence of seals extremely unlikely |
| Birkholzer et al., 2011 | • synthetic<br>• 12 $km^2$ (radial symmetric) | closed | TOUGH2/EOS7 | Simulated by pressure build-up | – | Brine migration up a leaking wellbore | • Continuous flow only occurs if pressure perturbation in the reservoir is large enough to overcome the increased weight of the fluid column |
| Nicot (2008) | • Gulf Coast, USA<br>• 80 000 $km^2$ | closed | MODLFLOW96 | 50 and 250 $Mt\,yr^{-1}$ over 50 years | Water | Pressure build-up and migration of brine in the reservoir and through low permeable caprocks | • Average water table rise is in the same order of magnitude as seasonal and inter-annual variations |
| Oldenburg and Rinaldi (2011) | • synthetic<br>• 1 km (2-D) | closed | TOUGH2/EOS7 | Simulated by pressure build-up | – | Brine displacement in shallower aquifers through a vertical conduit (borehole or fault) | • Depending on brine density and pressure gradient fluid migrates upward until a new static steady-state equilibrium is reached or a sustained flow develops, if the brine is allowed to spread laterally. |
| Tillner et al. (2013) | • North German Basin<br>• 1 764 $km^2$ | closed and open | TOUGH2-MP/ECO2N | 1.7 $Mt\,yr^{-1}$ over 20 years | $CO_2$ | Brine migration through faults dependent on reservoir compartmentalisation and fault permeability | • Degree of pressurization is the driving mechanism for brine migration<br>• Permeability of fault zones does not influence salinization of shallower aquifers significantly |
| Yamamoto et al., 2009 | • Bay of Tokyo, Japan<br>• 4 200 $km^2$ | open | TOUGH2-MP/ECO2N | 10 $Mt\,yr^{-1}$ over 100 years | $CO_2$ | Pressure build-up and brine migration in the reservoir and through low permeable caprocks | • Pressure build-up of a few bars can occur in the shallow confined aquifers over extensive regions |
| Zhou et al. (2010) | • Illinois basin, USA<br>• 241 000 $km^2$ | open | TOUGH2-ECO2N | 100 $Mt\,yr^{-1}$ over 50 years | $CO_2$ | Pressure build-up and brine migration in the reservoir and through low permeable caprocks | • Pressure build-up of 1 and 0.1 bar can be expected as far as 150 and 300 km from the injection area, respectively<br>• pressure increase of 35 bar at injection does not affect caprock integrity |
| This study | • North German Basin<br>• 10 000 $km^2$ | closed and open | TOUGH2-MP/ECO2N | 1.7 $Mt\,yr^{-1}$ over 20 years | Water | Brine migration through fault zones depending on different geological conditions | • Boundary conditions, fault length and existence of an overlying secondary reservoir affect pressure development in the reservoir and thereby freshwater salinization |





HESSD
12, 5703–5748, 2015

**Table 2.** Vertical grid discretization, depth and hydraulic parameters for the active geological units.

| Unit | $k$ (mD) | $\Phi$ (%) | thickness (m) | depth (m) | element layers | vertical resolution (m) |
|---|---|---|---|---|---|---|
| Rupelian basal sands | 1000 | 20 | 20 | −110 to −130 | 2 | 10 |
| Muschelkalk Formation | 200 | 20 | 140 | −1025 to −1165 | 7 | 19.9 |
| Detfurth Formation | 400 | 17 | 23 | −1425 to −1448 | 2 | 11.5 |
| Faults | 700 | 18.5 | | | 50 | 19.9 |





HESSD
12, 5703–5748, 2015

**Table 3.** Overview about all calculated scenarios, their mean reservoir pressures at the end of injection as well as depth of origin and distribution of the brine displaced into the shallow aquifer.

| Scenario | | | Duration of mass flow into the shallow aquifer[a] (yrs) | Mean Δp in the Detfurth Formation (bar)[b] | Lateral distance affected by salinity increase (km)[c] | | Upper part of the fault, where brine originates from (m)[c] | |
|---|---|---|---|---|---|---|---|---|
| | | | | | Max. | Min. | Max. | Min. |
| Closed reservoir boundaries | 2 layers | $F_1^{2\,km}$ $B_C$ | 330 | 19.4 | 6.1 | – | 298 | – |
| | | $F_1^{60\,km}$ $B_C$ | 115 | 8.2 | 2.4 | 1.5 | 32 | 10 |
| | | $F_{1-4}^{193\,km}$ $B_C$ | 66 | 4.6 | 2.4 | 1.2 | 30 | 3 |
| | 3 layers | $F_1^{2\,km}$ $B_C SR_{200\,mD}$ | 1050 | 15.9 | 6.1 | – | 265 | – |
| | | $F_1^{60\,km}$ $B_C SR_{200\,mD}$ | 390 | 5.2 | 2.4 | 2 | 20 | 7 |
| | | $F_{1-4}^{193\,km}$ $B_C SR_{200\,mD}$ | 225 | 2.9 | 2 | 1.5 | 19 | 3 |
| Open reservoir boundaries | 2 layers | $F_1^{2\,km}$ $B_O$ | 31 | 3.5 | 4 | – | 108 | – |
| | | $F_1^{60\,km}$ $B_O$ | 31 | 2.2 | 2.2 | 0.95 | 29 | 2 |
| | | $F_{1-4}^{193\,km}$ $B_O$ | 42 | 2.1 | 2.2 | 0.95 | 28 | 2 |
| | 3 layers | $F_1^{2\,km}$ $B_O SR_{200\,mD}$ | 31 | 3.2 | 2.8 | – | 59 | – |
| | | $F_1^{60\,km}$ $B_O SR_{200\,mD}$ | 40 | 1.6 | 1.7 | 0.95 | 17 | 1 |
| | | $F_{1-4}^{193\,km}$ $B_O SR_{200\,mD}$ | 45 | 1.3 | 1.7 | 0.95 | 17 | > 1 |
| | | $F_{1-4}^{193\,km}$ $B_O SR_{2000\,mD}$ | 23 | 0.6 | 1.1 | 0.35 | 4 | > 1 |

[a] total mass flow $> 0.1\,kg\,s^{-1}$,
[b] $t$ = 20 years,
[c] $t$ = end of mass flow.





HESSD
12, 5703–5748, 2015

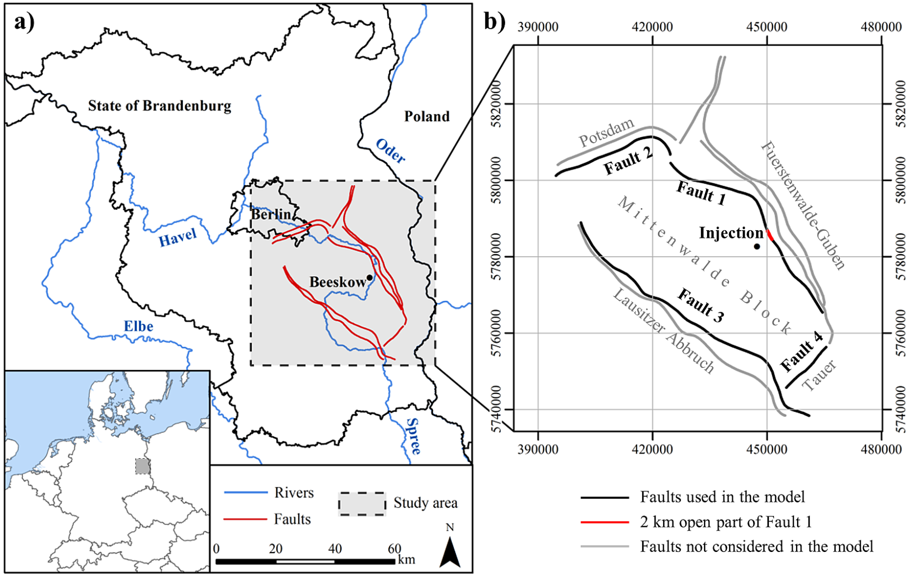


**Figure 1. (a)** Dashed rectangle indicates the location of the study area in the State of Brandenburg (Germany), while red lines illustrate the present fault systems. **(b)** Only the inner faults (black lines), facing to the injection well, were implemented to represent the entire fault zone. Axes show UTM-coordinates (WGS84/UTM zone 33N). Rivers and the outline of the states of Brandenburg and Berlin were derived from Tillner et al. (2013).





HESSD

12, 5703–5748, 2015

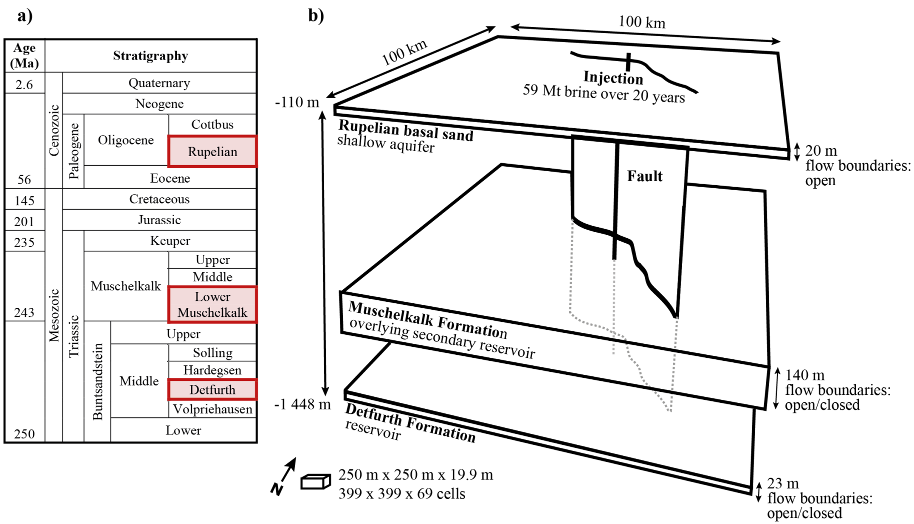


**Figure 2. (a)** Stratigraphy of the study area with the active model layers highlighted in red. **(b)** The geological 3-D model with simplified topography comprises up to three layers.





HESSD
12, 5703–5748, 2015

Effective damage zone volume of fault zones and initial salinity distribution

M. Langer et al.

Title Page
Abstract
Introduction
Conclusions
References
Tables
Figures
◀I
▶I
◀
▶
Back
Close
Full Screen / Esc
Printer-friendly Version
Interactive Discussion

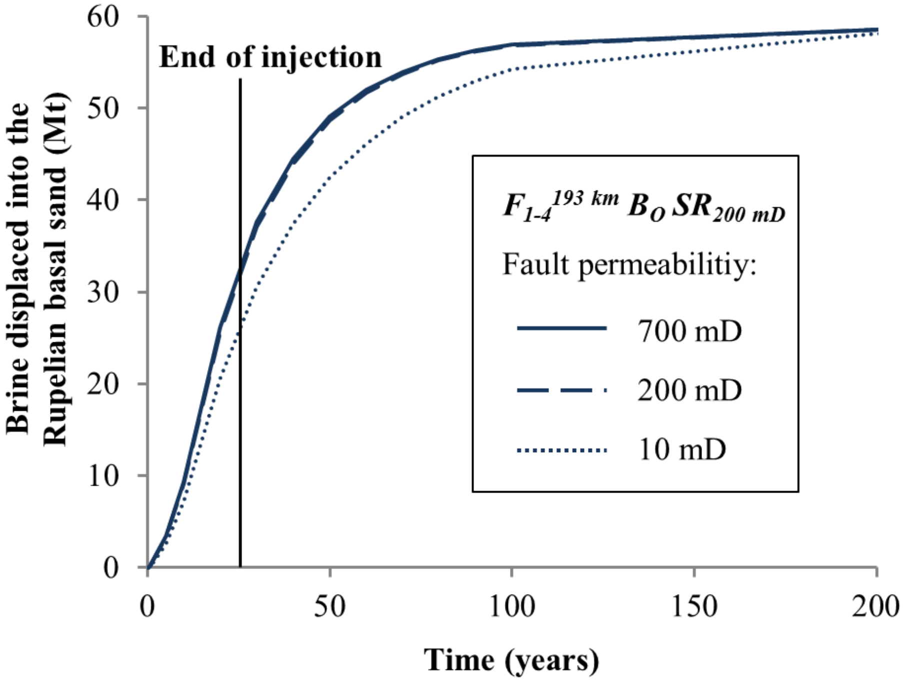


**Figure 3.** Temporal evolution of brine displacement into the Rupelian basal sands, when all four faults are open, a secondary overlying reservoir exists and reservoir boundaries are closed. The brine mass displaced into the shallow aquifer is equal for all scenarios after 200 years, irrespective whether the fault permeability is higher (solid line), equal (dashed line) or lower (dotted line) to the permeability of the secondary reservoir. Lower fault permeabilities lead to retardation in mass flow only.





HESSD
12, 5703–5748, 2015

Effective damage zone volume of fault zones and initial salinity distribution

M. Langer et al.

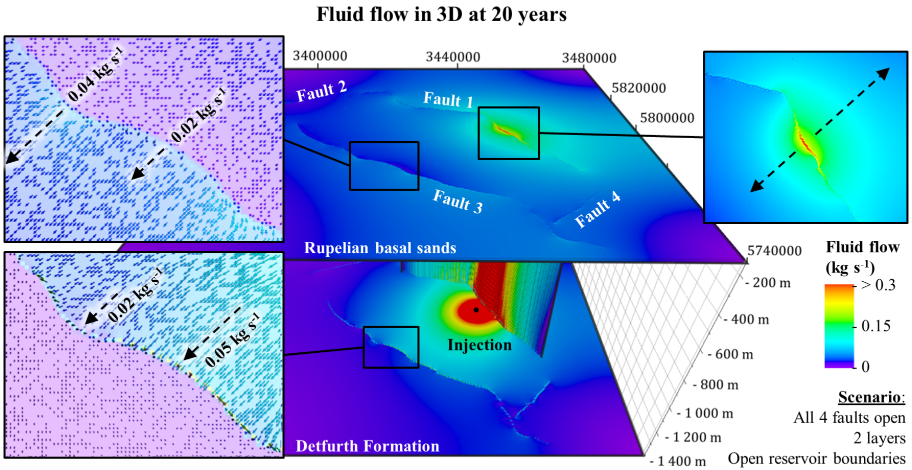


**Figure 4.** An injection-related pattern in fluid flow, as illustrated for Scenario $F_{1-4}^{193\,\mathrm{km}}\,B_{\mathrm{O}}$, is observed in all simulations. Within the reservoir, brine is displaced predominantly into parts of the faults lying closer to the injection well. It is the opposite in the shallow aquifer, where flow out of the fault is greater into parts not facing towards the injection.





HESSD
12, 5703–5748, 2015

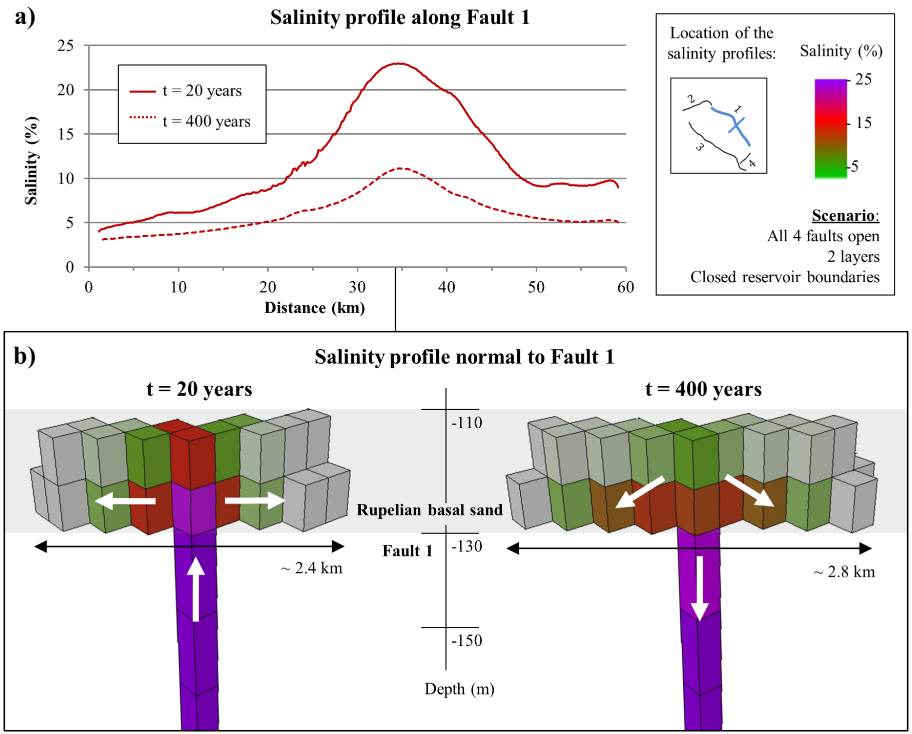


**Figure 5. (a)** Profile along Fault 1 ($F_{1-4}^{193\,\mathrm{km}}\ B_\mathrm{C}$) shows highest salinities near to the injection well. A decrease in salinization due to a downward flow is observed for the time after the injection period. **(b)** Cross section normal to Fault 1 illustrates the propagation of the saltwater plume (salinities > 0.05 %), while higher salinities can be observed within the lower element layer. White arrows illustrate schematically the direction of the fluid flow at 20 and 400 years.



HESSD
12, 5703–5748, 2015

Effective damage zone volume of fault zones and initial salinity distribution

M. Langer et al.

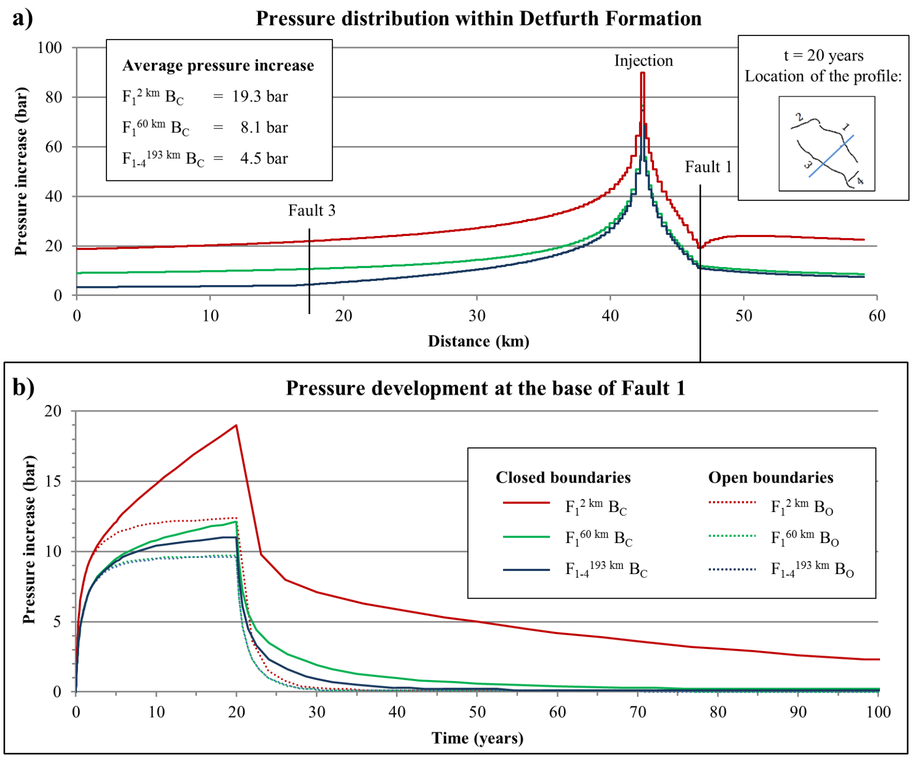


**Figure 6. (a)** Distribution of the pressure increase within the Detfurth Formation along the highlighted cross section significantly varies depending on the open fault length. Highest pressurization is observed for a short fault ($F_1^{2\,\mathrm{km}}\,B_C$). **(b)** Pressure development at the base of Fault 1 indicates a substantially faster pressure reduction for greater fault lengths.





HESSD
12, 5703–5748, 2015

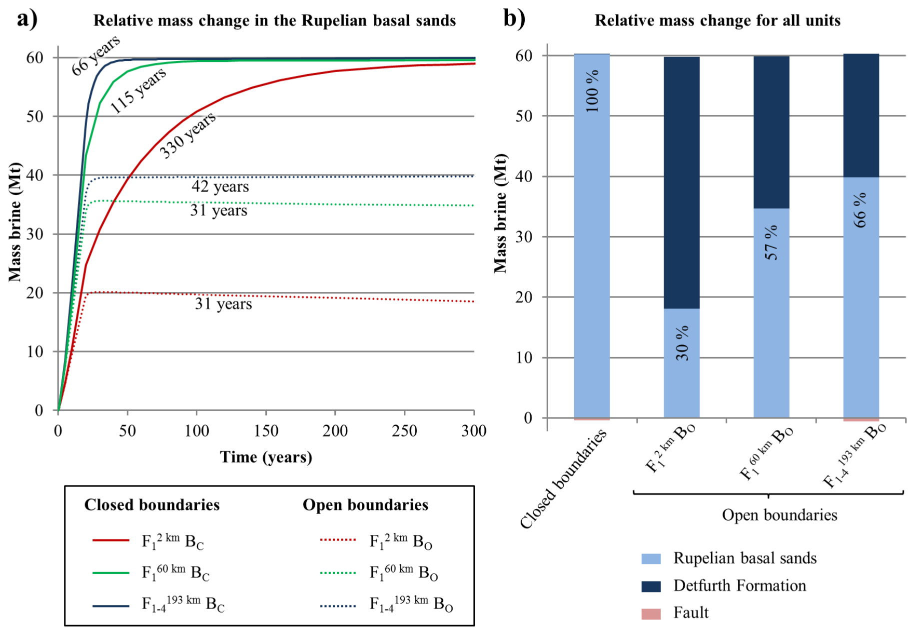


**Figure 7. (a)** Relative mass change in the Rupelian basal sands shows that the mass of brine displaced into the shallow aquifer corresponds to the overall injected fluid mass, if reservoir boundaries are closed. As indicated by the duration of mass flow (black numbers), only a temporal effect on fluid migration occurs. **(b)** Relative mass change for all lithological units after 330 years (mass flow $< 0.1\ kg\,s^{-1}$ for all scenarios) illustrates a considerably reduced salinization of the Rupelian basal sands for open reservoir boundaries.





HESSD
12, 5703–5748, 2015

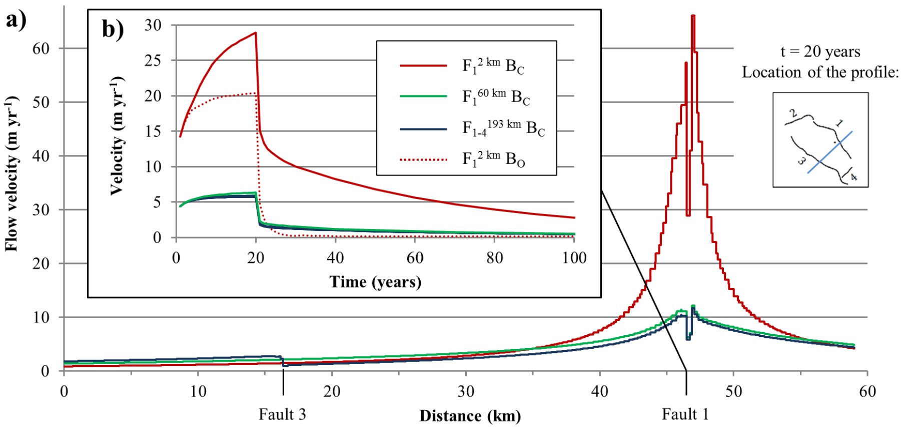


**Figure 8. (a)** Velocity profile within the lower element layer of the Rupelian basal sands shows highest flow velocities out of Fault 1 at the end of injection period. **(b)** Flow velocities out of Fault 1 increase until the end of the injection period (20 years) and decrease afterwards depending on pressure reduction of the respective scenarios.





HESSD

12, 5703–5748, 2015

Effective damage zone volume of fault zones and initial salinity distribution

M. Langer et al.

Title Page
Abstract | Introduction
Conclusions | References
Tables | Figures
◂◂ | ▸▸
◂ | ▸
Back | Close
Full Screen / Esc
Printer-friendly Version
Interactive Discussion

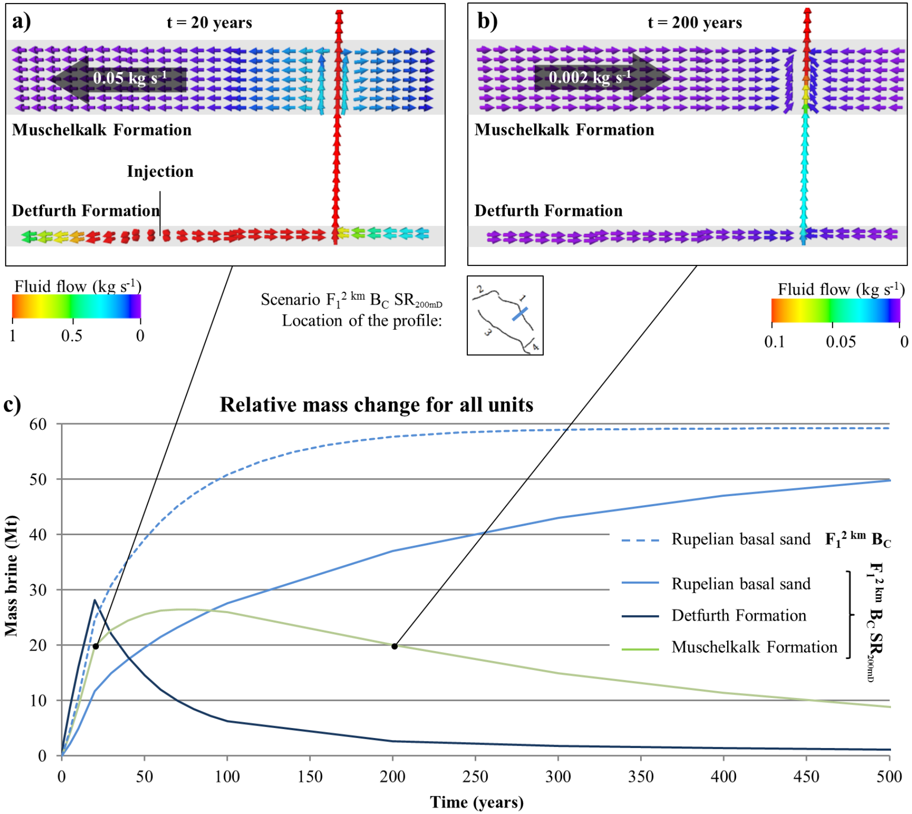


**Figure 9. (a)** Cross profile normal to Fault 1 shows, that during the injection period the displaced fluid spreads within the Detfurth and the Muschelkalk. **(b)** Afterwards, brine is transported out of the respective reservoir due to pressure reduction in both reservoirs. **(c)** Temporal evolution of the relative mass change shows the resulting retardation in fluid flow into the Rupelian basal sands for scenario $F_1^{2\,\mathrm{km}}\ B_\mathrm{C}\mathrm{SR}_{200\,\mathrm{mD}}$.





HESSD
12, 5703–5748, 2015

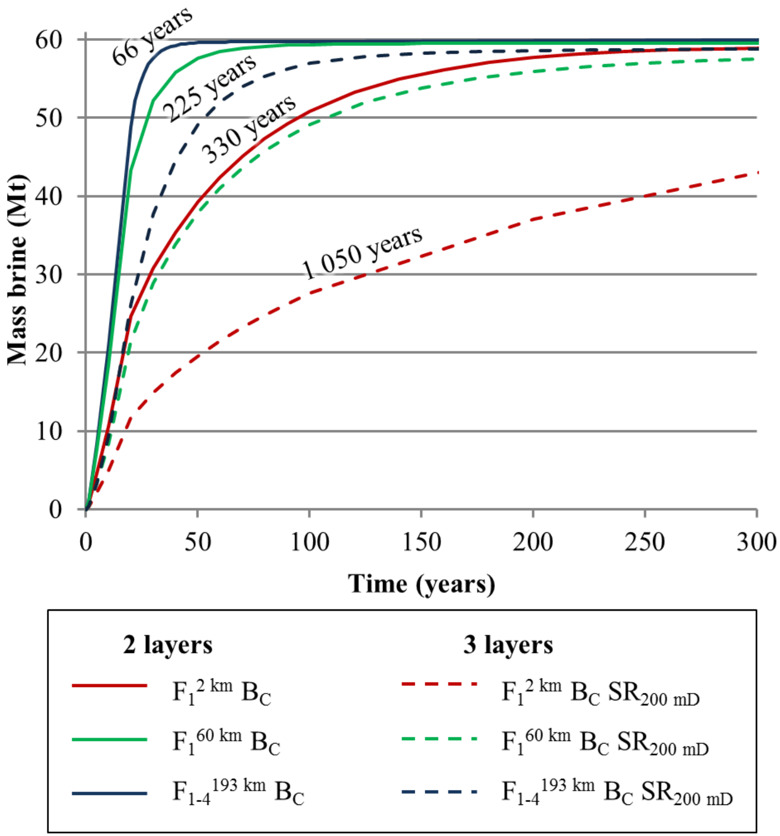


**Figure 10.** Relative mass change of the Rupelian basal sands illustrates the retardation in fluid flow (black numbers) due to the existence of an overlying reservoir, while the overall displaced brine mass into the shallow aquifer is almost identical, when pressure comes to equilibrium.





HESSD
12, 5703–5748, 2015
Effective damage zone volume of fault zones and initial salinity distribution
M. Langer et al.

Title Page
Abstract | Introduction
Conclusions | References
Tables | Figures
◂ | ▸
Back | Close
Full Screen / Esc
Printer-friendly Version
Interactive Discussion

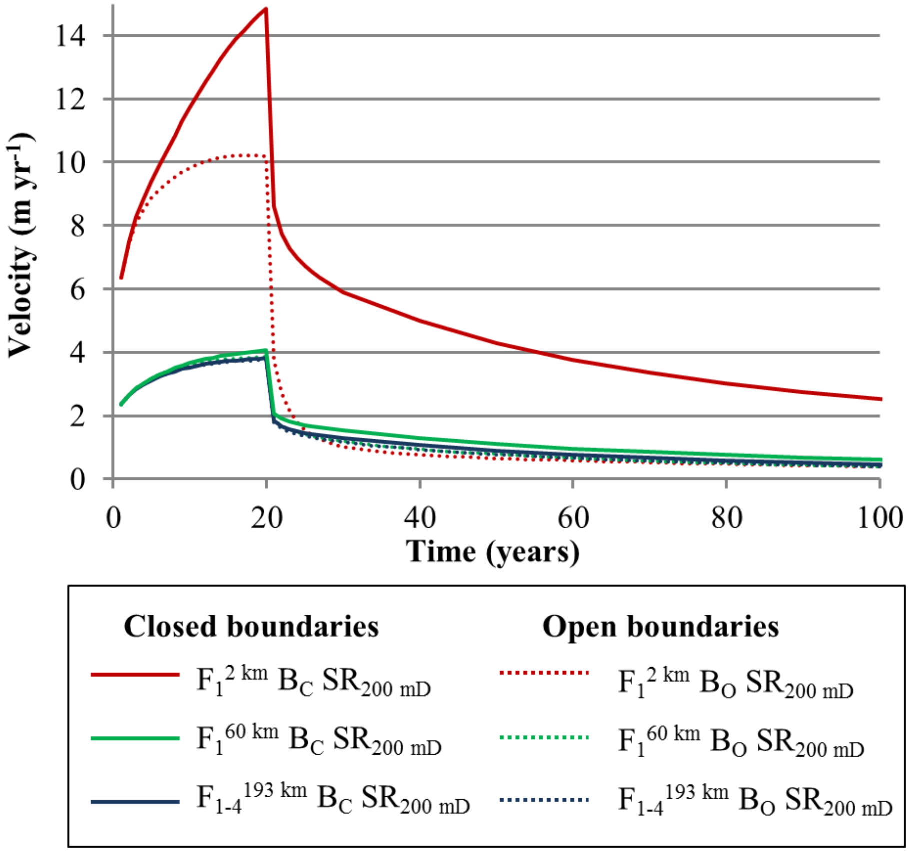


**Figure 11.** The temporal evolution of the flow velocities out of Fault 1 show a substantial reduction due to lower reservoir pressures for the scenarios considering a secondary overlying reservoir as well as open boundaries.





HESSD
12, 5703–5748, 2015

Effective damage zone volume of fault zones and initial salinity distribution

M. Langer et al.

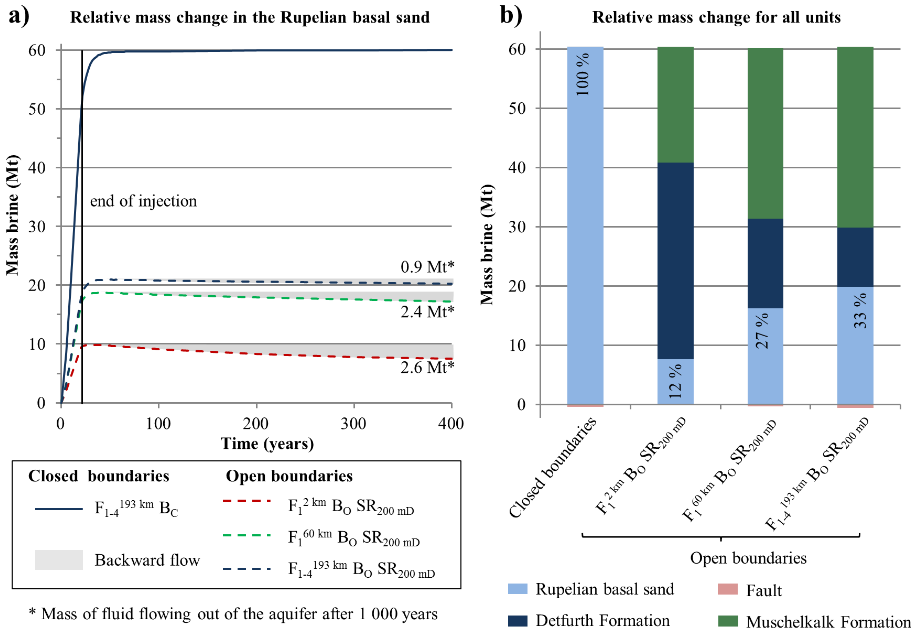


**Figure 12. (a)** Temporal evolution of the relative mass change of the Rupelian basal sands shows a lower duration of mass flow for open reservoir boundary conditions. Further a slight backward flow out of the aquifer can be observed. **(b)** Relative mass change for lithological units at 1000 years (considering the backflow) illustrates, that salinization in the shallow aquifer is substantially reduced, if reservoir boundaries are open, and further an overlying secondary reservoir exists.





HESSD
12, 5703–5748, 2015

Effective damage zone volume of fault zones and initial salinity distribution

M. Langer et al.

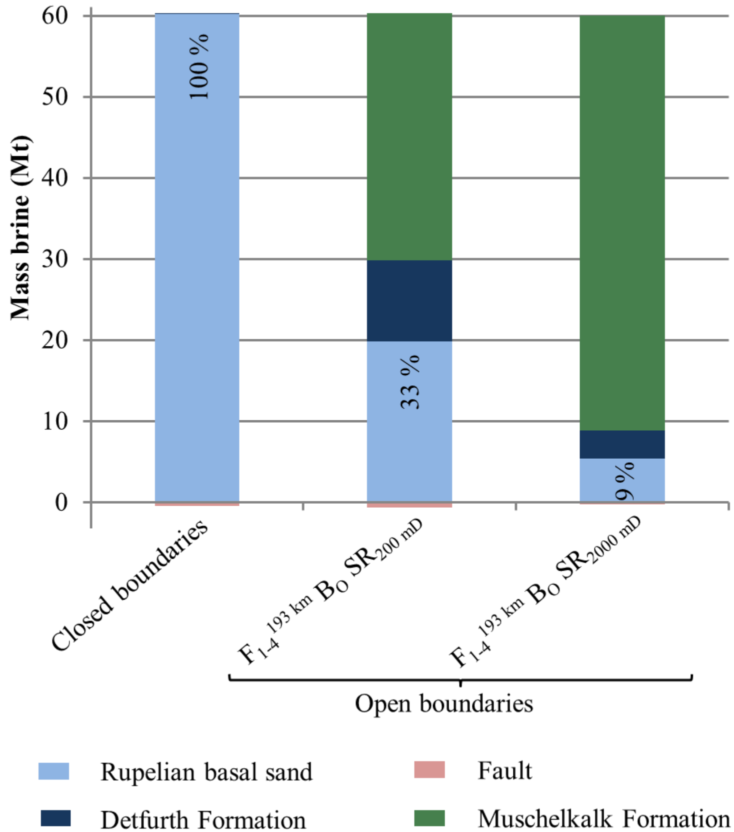


**Figure 13.** Relative mass change for all lithological units after 1000 years (considering the backflow) illustrates that if permeability of the fault is lower than of the Muschelkalk Formation ($F_{1-4}^{193\,\mathrm{km}}$ $B_O\mathrm{SR}_{2000\,\mathrm{mD}}$) brine is preferentially displaced into the overlying secondary reservoir. Consequently, freshwater salinization in the shallow aquifer is lowest compared to all other scenarios.





HESSD

12, 5703–5748, 2015

Effective damage zone volume of fault zones and initial salinity distribution

M. Langer et al.

Title Page
Abstract Introduction
Conclusions References
Tables Figures
◀ ▶
Back Close
Full Screen / Esc
Printer-friendly Version
Interactive Discussion